Effects of off-stoichiometry on the spin polarization at the $Co_2Mn_\beta Ge_{0.38}$/MgO interfaces: X-ray magnetic circular dichroism study

V. R. Singh,[1,*] V. K. Verma,[1] K. Ishigami,[1] G. Shibata,[1] T. Kadono,[1] A. Fujimori,[1] D. Asakura,[2] T. Koide,[2] Y. Miura,[3] M. Shirai,[3] G.-f. Li,[4] T. Taira,[4] and M. Yamamoto[4]

[1]*Department of Physics, University of Tokyo, Bunkyo-ku, Tokyo 113-0033, Japan*

[2]*Photon Factory, IMSS, High Energy Accelerator Research Organization, Tsukuba, Ibaraki 305-0801, Japan*

[3]*Research Institute of Electrical Communication, Tohoku University, Katahira 2-1-1, Aoba-ku, Sendai 980-8577, Japan*

[4]*Division of Electronics for Informatics, Hokkaido University, Sapporo 060-0814, Japan*

(Received 19 July 2012; published 19 October 2012)

We have studied the electronic and magnetic states of Mn and Co atoms at the $Co_2Mn_\beta Ge_{0.38}$ (CMG)/MgO ($\beta = 0.67$–1.8) interfaces, which constitute CMG/MgO/CMG magnetic tunnel junctions, by means of x-ray absorption spectroscopy (XAS) and x-ray magnetic circular dichroisms (XMCDs) at the Mn and Co $L_{2,3}$ edges and compared the deduced Co and Mn magnetic moments by the density-functional calculations with the coherent potential approximation (CPA). As the Mn content β increased, the intensity of Mn $L_{2,3}$ XMCD decreased, in agreement with the result of the CPA calculation, which showed the resultant reduction of charges and spin moment on Mn atoms because of the delocalization of Mn $3d$ electrons with increasing β. The Co spin magnetic moment for all the samples increased with decreasing β, again consistent with the present calculation and the previous density-functional calculation by Picozzi *et al.* that the Co_{Mn} antisite has a larger magnetic moment than that of Co atoms at the regular sites and reduces the spin polarization at the Fermi level and hence the tunnel magnetoresistance ratio.

DOI: 10.1103/PhysRevB.86.144412 PACS number(s): 75.70.−i, 68.35.Ct, 75.50.Cc, 73.20.−r

I. INTRODUCTION

Materials which exhibit half-metallic ferromagnetism have recently attracted great interest because a high efficiency is expected for spintronic device applications, including tunnel magnetoresistance (TMR) devices[1–3] and giant magnetoresistance devices.[4] In these materials the majority spin states have a metallic character with a nonzero density of states (DOS) at the Fermi level, while the minority spin states have a band gap at the Fermi level, resulting in 100% spin polarization at the Fermi level (E_F). To date there are many materials predicted to be half-metals at room temperature, and among them, the $L2_1$ ordered full Heusler alloys Co_2MnSi and Co_2MnGe are promising candidate for spintronics applications due to their high Curie temperatures, 985 K for Co_2MnSi and 905 K for Co_2MnGe.[5] For spin-transport processes it is interface rather than bulk properties that are of essential importance, because the TMR ratio is sensitive to the interfaces.[6]

Off-stoichiometry of the Heusler alloys is also expected to profoundly influence the half-metallic ferromagnetism and hence the TMR characteristic. The effect of defects in the Heusler alloys Co_2YZ introduced by off-stoichiometry on the spin-dependent electronic structure has been investigated theoretically[7–12] as well as experimentally.[13–15] Picozzi *et al.*[7] have predicted from a first-principles calculation that half-metallicity in Co_2MnSi and Co_2MnGe is lost by Co_{Mn} antisites through the appearance of minority-spin in-gap states around E_F, while half-metallicity is robustly retained by Mn_{Co} antisites. The calculation has also predicted that Mn_{Co} is coupled antiferromagnetically with neighboring Co atoms and that Co_{Mn} has a larger magnetic moment than Co atoms at the regular sites. Ishikawa *et al.*[14] and Yamamoto *et al.*[15] have made systematic studies of the effect of nonstoichiometry of Heusler alloy thin films on the spin-dependent tunneling characteristics of Co_2MnZ/MgO/Co_2MnZ (Z = Si, Ge) magnetic tunnel junctions (MTJs) and found that a higher TMR ratio is obtained for Mn compositions $\alpha > 1.0$ in $Co_2Mn_\alpha Si$ electrodes and, similarly, for Mn compositions $\beta > 1.0$ in Ge-deficient $Co_2Mn_\beta Ge_\delta$ electrodes (where $\delta < 1$). The observed lower TMR ratios for MTJs with Mn-deficient $Co_2Mn_\alpha Si$ or $Co_2Mn_\beta Ge_\delta$ electrodes were explained by the formation of Co_{Mn} antisites that lead to minority-spin in-gap states around E_F as theoretically predicted by Picozzi *et al.*[7] Furthermore, the observed higher TMR ratio for MTJs with Mn-rich $Co_2Mn_\alpha Si$ or $Co_2Mn_\beta Ge_\delta$ electrodes was explained by suppressed Co_{Mn} antisites, which caused a reduced density of minority-spin in-gap states around E_F.[14,15] Therefore, it is important to further investigate experimentally the effect of structural defects associated with nonstoichiometry on the electronic and magnetic properties in Co-based Heusler-alloy electrodes, particularly in the interfacial region between the Co_2YZ electrode and the tunnel barrier.

In order to investigate the magnetic properties of various atomic defects, element-specific x-ray absorption spectroscopy (XAS) and x-ray magnetic circular dichroism (XMCD) are proven to be most powerful techniques. Because of the shallow probing depths, these techniques are effective for study of the electronic and magnetic properties of interfaces, which play important roles in TMR devices. To date several studies have utilized these techniques to examine the interfacial properties of materials used in MTJs,[16–24] and some of them have focused on Heusler-alloy-based MTJs. Electronic and magnetic properties at interfaces have been investigated for various thicknesses in Co-rich Co_2MnSi[25,26] and Co_2MnGe[27] thin films. However, so far, element-specific studies of the effects of off-stoichiometry in Heusler-alloy thin films on their electronic and magnetic properties have not been carried out. In this paper, we have studied element specifically how the electronic and magnetic states of Mn and Co atoms in Ge-deficient $Co_2Mn_\beta Ge_{0.38}$ (CMG) facing an MgO barrier are

affected by nonstoichiometry by using XAS and XMCD and a density-functional calculation. The calculation was made for a wide range of nonstoichiometry corresponding to the real material $Co_2Mn_\beta Ge_\delta$ with $0.6 < \beta < 1.8$ and $\delta \sim 0.4$,[15] which exceeds the range studied by Piccozi *et al.*,[7] where the properties of a single antisite defect are dominant.

II. METHODS

In order to extract information about the interfacial magnetic and electronic states of CMG/MgO half-MTJs, we prepared films with various βs in CMG electrodes. The sample layer structure which we studied was as follows: (from the substrate side) MgO buffer layer (10 nm)/CMG (30 nm)/MgO barrier (2 nm)/AlO_x (1 nm) cap, grown on a MgO(001) substrate as shown in Fig. 1. All layers were successively deposited in an ultrahigh-vacuum chamber (with a base pressure of $\sim 6 \times 10^{-8}$ Pa) through radio-frequency (rf)-magnetron sputtering for CMG and electron beam evaporation for MgO. The CMG films were deposited at room temperature by rf-magnetron cosputtering from a stoichiometric CMG target and a Mn target, and the films deposited on the MgO buffer were subsequently annealed *in situ* at 500°C for 15 min. The preparation of the samples has been described in detail elsewhere.[15] Reflection high-energy electron diffraction measurements clearly showed that both the cosputtered CMG electrode and the MgO barrier in the CMG/MgO half-junction grew epitaxially.[14] Microbeam electron diffraction patterns indicated that a Mn-rich CMG film with a film composition of $Co_2Mn_{1.20}Ge_{0.38}$ prepared by cosputtering had the B2 structure.[28] Furthermore, high-resolution transmission electron microscopy (HRTEM) images of a CMG/MgO/CMG MTJ trilayer with cosputtered CMG films clearly showed that all the layers in the MTJ trilayer were grown epitaxially and were single crystalline.[28] The HRTEM lattice images also confirmed that extremely smooth and abrupt interfaces were formed for the MTJ tailayer. Thus, it was confirmed that identically prepared CMG/MgO half-junctions featured extremely smooth and abrupt interfaces.

XAS and XMCD measurements were performed at BL-16A of the Photon Factory. The monochromator resolution was $E/\Delta E > 10\,000$. The degree of circular polarization of x rays was $87\% \pm 4\%$. The base pressure of the chamber was about 1×10^{-9} Torr. XAS and XMCD spectra were obtained without any surface treatment in the total electron yield mode, whose probing depth is ~5 nm. XMCD was measured with magnetic fields (±3 T) applied perpendicular to the film surfaces at 20 and 300 K.

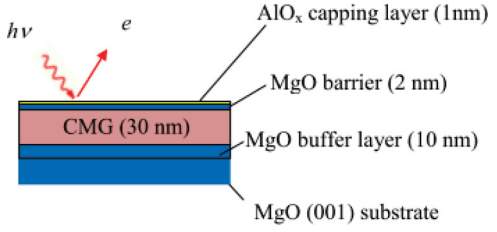

FIG. 1. (Color online) Schematic layer structure of CMG/MgO thin film samples.

TABLE I. Films with Mn compositions β in the expression of $Co_2Mn_\beta Ge_{0.38}$ and site occupancies of the CMG samples used in the present study.

β	Site occupancy
0.67	$Co_2[Mn_{0.377}Co_{0.623}][Ge_{0.498}Mn_{0.502}]$
0.85	$Co_2[Mn_{0.523}Co_{0.477}][Ge_{0.471}Mn_{0.529}]$
1.03	$Co_2[Mn_{0.654}Co_{0.346}][Ge_{0.446}Mn_{0.554}]$
1.20	$Co_2[Mn_{0.765}Co_{0.235}][Ge_{0.425}Mn_{0.575}]$
1.40	$Co_2[Mn_{0.884}Co_{0.116}][Ge_{0.402}Mn_{0.598}]$
1.60	$Co_2[Mn_{0.990}Co_{0.010}][Ge_{0.382}Mn_{0.618}]$
1.80	$[Co_{1.914}Mn_{0.086}]Mn[Ge_{0.364}Mn_{0.636}]$

Because Picozzi *et al.*'s[7] calculation was for stoichiometries only down to $Mn_{0.9}$ and $Ge_{0.9}$, we performed the density-functional calculations on the basis of the Korringa-Kohn-Postoker (KKR) method[29,30] with the coherent potential approximation (CPA) for a wider range of nonstoichiometries in Ge-deficient CMG. We used the generalized gradient approximation[31] for the exchange and correlation term. We adopted the experimental lattice constants obtained for the cosputtered cubic CMG thin films depending on the Mn composition β in CMG.[28] The KKR-CPA calculation was done on the most plausible model in which the deficient Ge sites are fully occupied by Mn atoms[15] as reported in Table I. In the present model, because no Mn atoms can occupy the Co sites to form Mn_{Co} antisites except for the largest β value, Picozzi *et al.*'s[7] argument that Mn_{Co} antisites antiferromagnetically coupled to the regular Mn spin reduce the average Mn spin moment does not apply to the entire range of the present sample compositions.

III. RESULTS AND DISCUSSION

Figure 2(a) shows the photon-flux-normalized polarization-dependent XAS spectra (μ_+ and μ_-) at the Mn $L_{2,3}$ edges ($2p_{3/2,1/2} \rightarrow 3d$ absorption edges) of CMG. Figure 2(b) displays the Mn $L_{2,3}$ edge XMCD ($\Delta\mu = \mu_+ - \mu_-$) spectra. Here, μ_+ and μ_- stand for the absorption coefficient for the photon helicity parallel and antiparallel to the Mn $3d$ majority spin. A linear plus two-step-like background has been subtracted from each XAS spectrum.[32] Here we note that another source of the error bar may come from this background subtraction. In the XAS spectra for $\beta = 0.67$ to 1.80, a shoulder-like structure is observed on the higher energy side of the Mn L_3 peak, and the Mn L_2 peak is split into a doublet. These features are characteristics observed for Co_2MnSi and Co_2MnGe.[33] In the XAS spectra for $\beta = 1.40$, 1.60, and 1.80, multiple fine structures were observed, implying that some of the interfacial Mn atoms are oxidized to Mn^{2+} as reported in the previous work.[27] Therefore, we have subtracted the oxide component Mn^{2+}-like multiplet structures such as MnO from the raw data for the $\beta = 1.40$, 1.60, and 1.80 films, as described in detail in the Appendix. The bulk properties of these films could be different from those of the interfacial region. XCMD depth profile studies by Amemiya *et al.*[34,35] suggest that the magnetic properties of only one to two monolayers are different from those of the bulk. Since our total electron yield mode has a probing depth of several nanometers,

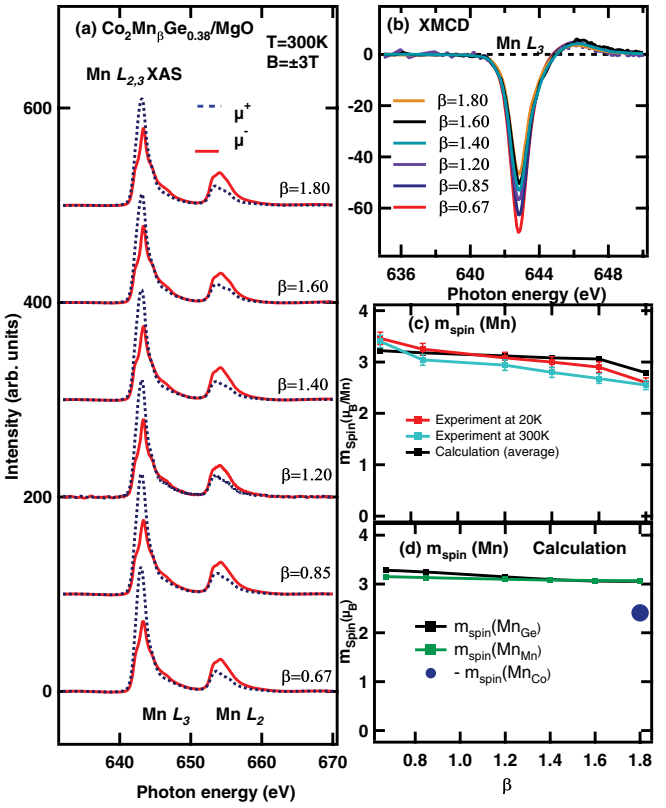

FIG. 2. (Color online) Mn $L_{3,2}$-edge XAS and XMCD of CMG samples with various Mn compositions (a) XAS taken at 300 K and $B = \pm 3$ T. μ_+ and μ_- are the absorption coefficients for photon helicity parallel and antiparallel to the Mn $3d$ majority spin, respectively. (b) XMCD spectra. (c) Mn composition (β) dependence of the Mn spin magnetic moment deduced using the sum rules[36,37] compared with that given by the KKR-CPA calculation. (d) β dependence of the Mn spin magnetic moment at different sites deduced from the density-functional calculation.

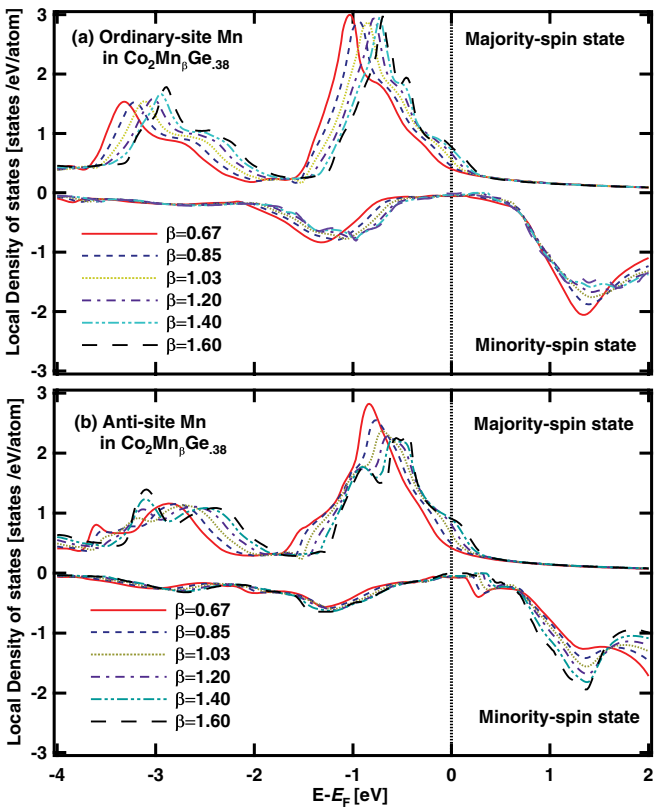

FIG. 3. (Color online) Local density of states for Mn at the regular site (a) and the antisite Mn (b) of $Co_2Mn_\beta Ge_{0.38}$ as functions of energy relative to the E_F.

signals of more than 70% come from the bulk. To confirm the bulk properties by XMCD, one has to do experiment in the total florescence yield mode, whose probing depth is ~100 nm.

The XMCD intensity at both 20 and 300 K decreases with β. By applying the sum rules to the XAS and XMCD spectra,[36,37] we have obtained the spin and orbital magnetic moments of the Mn atom. We have assumed that the contribution of the dipole operator term T_z in the spin sum rule is negligibly small because the Mn site in bulk CMG has T_d symmetry.[27] Since the L_3 and L_2 regions in Mn $L_{2,3}$ XAS and XMCD overlap due to the strong exchange interaction between the Mn $2p$ core hole and the Mn $3d$ electrons, we have divided the obtained spin magnetic moment by the correction factor 0.68 given by Teramura *et al.*[38] We have assumed a $3d$ hole number (n_h) of 4.5 for Mn[20,24,27] on the basis of the band structure calculations. The spin magnetic moment $m_{\rm spin}$ (Mn) thus deduced is plotted as a function of β in Fig. 2(c) and compared with the present KKR-CPA calculation. It is in the range of 2.6–3.4 μ_B, decreases slightly as the temperature increases from 20 to 300 K, and decreases weakly with increasing β, in good agreement with the KKR-CPA calculation. The decrease in $m_{\rm spin}$ (Mn) with increasing β is also consistent with the present calculation. The Mn orbital magnetic moment $m_{\rm orb}$ (Mn) (not shown) was found to be in the range 0.2 ± 0.005 to 0.3 ± 0.006 μ_B for all samples. Figure 2(d) shows the β dependence of the Mn spin magnetic moment at different sites deduced from the KKR-CPA calculation. Here, the magnetic moment of Mn at the regular site, $m_{\rm spin}(\rm Mn_{Mn})$, and that at the Ge site, $m_{\rm spin}(\rm Mn_{Ge})$, show almost the same behavior of a weak decrease with β, because the Mn atoms at both the regular-site and the Ge antisite lose charges in the majority-spin state. To confirm this, we show in Fig. 3 the local density of states (LDOS) of Mn $3d$ in CMG at both the regular-site and the Ge antisite. It is found that the LDOSs of Mn $3d$ shift toward the higher energy side with increasing β, indicating the reduction of charges of Mn $3d$. This can be attributed to the delocalization of Mn $3d$ states due to the increase in nearest-neighbor hybridization of Mn $3d$ with the regular-site Co $3d$ with increasing β. Since the LDOSs of Mn $3d$ show nearly half-metallic electronic structures, the reduction of charge is significant in the majority-spin states. This leads to the decrease in the Mn spin moment at both the regular site and the Ge site. The experimentally observed sudden decrease in $m_{\rm spin}$(Mn) at $\beta = 1.80$ is due not to the $m_{\rm spin}(\rm Mn_{Mn})$ or $m_{\rm spin}(\rm Mn_{Ge})$, but to the negative value of $m_{\rm spin}(\rm Mn_{Co})$. According to the site occupation model employed here (Table I), only the $\beta = 1.80$ sample has a finite number of $\rm Mn_{Co}$ antisites and consistently shows a reduced average $m_{\rm spin}$(Mn).

Figures 4(a) and 4(b) show the photon-flux-normalized XAS and XMCD spectra at the Co $L_{3,2}$ edges. All samples

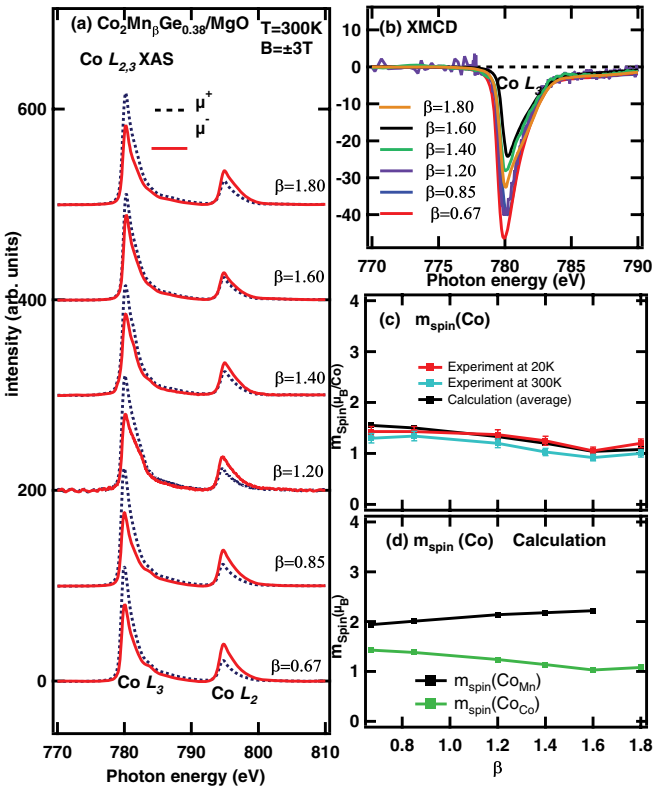

FIG. 4. (Color online) Co $L_{3,2}$-edge XAS and XMCD of CMG samples with various Mn compositions. (a) XAS taken at 20 and 300 K and $B = \pm 3$ T. μ_+ and μ_- are the absorption coefficients for photon helicity parallel and antiparallel to the Mn $3d$ majority spin, respectively. (b) XMCD spectra. (c) Mn composition (β) dependence of the Co spin magnetic moment deduced using the sum rules[36,37] compared with that given by the KKR-CPA calculation. (d) β dependence of the Co spin magnetic moment at different sites deduced from the density-functional calculation.

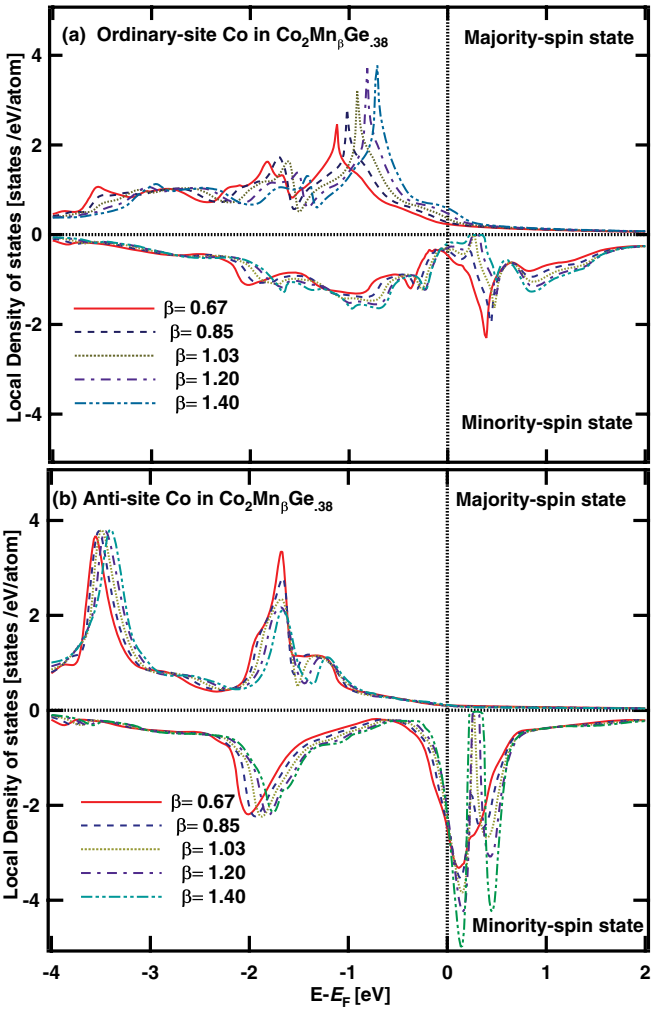

FIG. 5. (Color online) Local density of states for the ordinary-site Co (a) and the antisite Co (b) of $Co_2Mn_\beta Ge_{0.38}$ as functions of the energy relative to the E_F.

show a shoulder-like structure observed on the higher energy side of the Co L_3-edge XAS, common to thin film bulk samples.[27,33] Co-oxide-like multiplet structures[20] were not observed for any samples, meaning that Co atoms were not oxidized even in the interfacial region, consistent with the previous report.[27] To determine the Co magnetic moment, we again used the sum rules[36,37] assuming the $3d$ hole number (n_h) to be 2.2.[20,24,27] As shown in Fig 4(c), we experimentally determined the Co spin magnetic moment $m_{\rm spin}$(Co) to be in the range of 1.2 $\mu_{\rm B}$–1.4 $\mu_{\rm B}$, which is obviously larger than the theoretically predicted bulk value of 1.06 $\mu_{\rm B}$.[7,39] This can be explained by the presence of Co_{Mn} antisites, which are predicted to have larger spin magnetic moments than Co atoms at the regular sites. The decrease in $m_{\rm spin}$(Co) with increasing β in the experimental result can be understood as being due to the decreasing concentration of Co_{Mn} antisites and is also consistent with the present KKR-CPA calculation. The orbital magnetic moment $m_{\rm orb}$(Co) is relatively large despite the small $m_{\rm spin}$(Co), in the range of 0.2 ± 0.003 $\mu_{\rm B}$ to 0.3 ± 0.005 $\mu_{\rm B}$. Figure 4(d) shows the β dependence of the Co spin magnetic moment at different sites deduced from the KKR-CPA calculation. While the magnetic moment of Co at the regular site $m_{\rm spin}(Co_{Co})$ behaves similarly to the average Co moment, that of Co at the Mn site, $m_{\rm spin}(Co_{Mn})$, is much larger than the average Co moment and further increases with β. This is because, for large β, Co atoms at the Mn sites become dilute (Table I) and behave like isolated antisite Co atoms, which show an enhanced magnetic moment.[7] However, this increase in $m_{\rm spin}(Co_{Mn})$ is not reflected in the averaged $m_{\rm spin}$(Co) since the number of Co_{Mn} antisites decreases rapidly with β. The decrease in the spin moment of Co at the regular site $m_{\rm spin}(Co_{Co})$ is also attributed to the reduction in the majority-spin charge due to the delocalization of Co $3d$ states with increasing β. This can be confirmed by the LDOSs of Co $3d$ at the regular site in Fig. 5.

We have shown above that the deduced $m_{\rm spin}$(Mn) for the CMG samples decreases with Mn composition β. This result may be interpreted within the scenario that the Mn atoms at both the regular sites and the Ge sites lose charges with increasing β and the shift of the E_F to the lower energy side causes the reduction in the Mn spin moment. This mechanism was not considered by Picozzi *et al.*[7] because they did not study such a heavily off-stoichiometric region as in our CMG samples, in which a large amount of Mn fills the Ge deficiencies. On the other hand, the deduced $m_{\rm spin}$(Co) for all

the CMG samples is obviously larger than the theoretical value of the bulk sample, 1.06 μ_B, and the experimental XMCD value of 1.04 μ_B for the bulk samples reported by Miyamoto *et al.*[33] Picozzi *et al.*[7] theoretically investigated the effect of antisite defects in CMG and reported that the m_{spin}(Co) of the Co_{Mn} antisites in CMG was 1.35 μ_B, which was larger than the 1.06 μ_B for Co at the regular Co site. In the Co-rich region m_{spin}(Co) $\sim$ 1.20 μ_B, indicating the possible existence of Co_{Mn}. As described above, we showed experimentally a distinctly higher m_{spin}(Co) value, about 1.3 μ_B, for Co-rich samples than the theoretically predicted value of 1.06 μ_B for Co at the regular site,[7] and it is consistent with the higher m_{spin}(Co) value of 1.35 μ_B predicted theoretically for Co at the Mn site.[7] Thus, our element-specific spin-moment investigation along with the theoretical calculation demonstrates the existence of Co_{Mn} antisites for Co-rich CMG thin films. Furthermore, the experimental dependence of m_{spin}(Co) on β was in good agreement with the our theoretical result, and the decrease in m_{spin}(Co) with increasing β was explained by the decrease in the Co_{Mn} antisite ratio. The latter finding supports the understanding that Co_{Mn} antisites can be suppressed by a Mn-rich composition suggested by the β dependence of the TMR and saturation magnetization.[15] The calculated total DOS for each of the majority- and minority-spin states of CMG was reported by Picozzi *et al.*,[7] and in-gap states were found to exist within the minority-spin gap only when Co_{Mn} existed. That is, the existence of Co_{Mn} in CMG leads to a decrease in the spin polarization at the Fermi level. In fact, the spin polarization of Co-rich CMG estimated from the TMR ratio at 4.2 K was as low as 0.74.[40] Here, we note that the saturation magnetization (μ_s) value calculated assuming the Slater-Pauling rule for half-metallic Heusler alloys is close to the experimental μ_s value at $\beta = 1.40$.[15] The good agreement for $\beta = 1.40$ indicates that the Slater-Pauling rule is a good approximation for the CMG film with $\beta = 1.40$; that is, the CMG film with $\beta = 1.40$ is close to being half-metallic. This finding is also consistent with our XMCD and the KKR-CPA results as well as the observed high TMR ratios for CMG/MgO/CMG MTJs with $\beta = 1.40$.[15]

IV. CONCLUSION

In conclusion, we have studied the Mn concentration (β) dependence of the magnetic and electronic states of CMG/MgO interfaces by means of element-specific XMCD measurements and KKR-CPA calculation. The deduced m_{spin}(Mn) for all CMG samples decreased with β, consistent with the KKR-CPA calculation, which predicts that Mn atoms at both the regular sites and the Ge sites lose the magnitudes of the spin moment with β. The deduced m_{spin}(Co) values for all CMG samples are larger than the theoretical value of 1.06 μ_B for bulk stoichiometric CMG. In the Co-rich region, this can be explained by the existence of Co_{Mn} antisites that have a larger magnetic moment, m_{spin}(Co) $\sim$ 1.5 μ_B, which reduces the spin polarization at the Fermi level and decreases the TMR ratio. We have experimentally demonstrated through element-specific XMCD measurements, along with theoretical calculations, the existence of harmful Co_{Mn} antisites for Co-rich Co_2MnGe thin films and a decrease in the Co_{Mn} antisite ratio with increasing Mn composition, resulting in the improved half-metallicity.

ACKNOWLEDGMENTS

We would like to thank Kenta Amemiya and Masako Sakamaki for valuable technical support. This work was supported by a Grant-in-Aid for Scientific Research (No. S22224005) from the JSPS and the Quantum Beam Technology Development Program of the JST, Japan, and the Global COE Program of MEXT, Japan. The experiment at the Photon Factory was approved by the Program Advisory Committee (Proposal Nos. 2008G010, 2010G187, and 2010S2-001). The work at Hokkaido University was partly supported by a Grant-in-Aid for Scientific Research (A) (No. 23246055) from MEXT, Japan.

APPENDIX

For CMG/MgO samples with $\beta = 1.40$ to 1.80, the Mn L_3 edge XAS spectra showed additional fine structures because some of the Mn atoms at the interfaces were oxidized as reported in the previous work.[27] In order to subtract the Mn oxide contribution from the measured spectra, we have synthesized the spectra of Mn oxide (most likely a Mn^{2+} oxide) by subtracting the Mn L_3-edge XAS of the $\beta = 0.85$

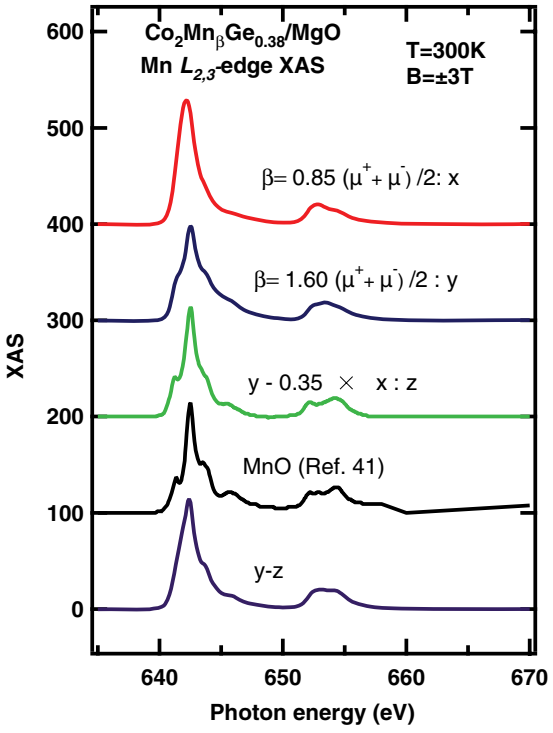

FIG. 6. (Color online) The top two curves show the Mn $L_{2,3}$-edge XAS of a CMG $\beta = 1.60$ sample (y) and that of a $\beta = 0.85$ sample (x). The green spectrum was obtained by subtracting an appropriate amount of the unoxidized $\beta = 0.85$ spectrum from the oxidized $\beta = 1.60$ data ($y - 0.3 \times x$). The black spectrum is the Mn $L_{2,3}$-edge XAS of MnO taken from Ref. 41. The bottom spectrum is the "intrinsic" Mn $L_{2,3}$-edge XAS spectrum of $\beta = 1.60$ without oxidation.

sample at 300 K, which would represent unoxidized Mn, from that of the $\beta = 1.60$ sample, as shown in Fig. 6. The subtraction was made so that the deduced spectrum becomes similar to the Mn L_3-edge XAS of MnO.[41] Because MnO is a paramagnetic insulator at room temperature and an antiferromagnetic insulator below $T_N \sim 120$ K, oxidized Mn atoms in the $\beta = 1.60$ sample would not contribute to the ferromagnetism.

*Corresponence author: vijayraj@wyvern.phys.s.u-tokyo.ac.jp

[1] S. Kammerer, A. Thomas, A. Hutten, and G. Reiss, Appl. Phys. Lett. **85**, 79 (2004).
[2] Y. Sakuraba, M. Hattori, M. Oogane, Y. Ando, H. Kato, A. Sakuma, T. Miyazaki, and H. Kubota, Appl. Phys. Lett. **88**, 192508 (2006).
[3] T. Ishikawa, T. Marukame, H. Kijima, K.-I. Matsuda, T. Uemura, M. Arita, and M. Yamamoto, Appl. Phys. Lett. **89**, 192505 (2006).
[4] K. Yakushiji, K. Saito, S. Mitani, K. Takanashi, Y. K. Takahashi, and K. Hono, Appl. Phys. Lett. **88**, 222504 (2006).
[5] P. J. Webster, J. Phys. Chem. Solids **32**, 1221 (1971).
[6] J. M. de Teresa, A. Barthlemy, A. Fert, J. P. Contour, F. Montaigne, and P. Seneor, Science **286**, 507 (1999).
[7] S. Picozzi, A. Continenza, and A. J. Freeman, Phys. Rev. B **69**, 094423 (2004).
[8] Y. Miura, K. Nagao, and M. Shirai, Phys. Rev. B **69**, 144413 (2004).
[9] I. Galanakis, K. Ozdogan, B. Aktas, and E. Sasioglu, Appl. Phys. Lett. **89**, 042502 (2006).
[10] K. Ozdogan, E. Sasioglu, and I. Galanakis, Phys. Status Solidi (RRL) **1**, 184 (2007).
[11] I. Galanakis, K. Ozdogan, E. Sasioglu, and B. Aktas, Phys. Status Solidi A **205**, 1036 (2008).
[12] B. Hulsen, M. Scheffler, and P. Kratzer, Phys. Rev. B **79**, 094407 (2009).
[13] T. Marukame and M. Yamamoto, J. Appl. Phys. **101**, 083906 (2007).
[14] T. Ishikawa, H.-x. Liu, T. Taira, K.-i. Matsuda, T. Uemura, and M. Yamamoto, Appl. Phys. Lett. **95**, 232512 (2009).
[15] M. Yamamoto, T. Ishikawa, T. Taira, G.-f. Li, K.- ichi Matsuda, and T. Uemura, J. Phys.: Condens. Matter **22**, 164212 (2010).
[16] J. Schmalhorst, M. Sacher, A. Thomas, H. Bruckl, G. Reiss, and K. Starke, J. Appl. Phys. **97**, 123711 (2005).
[17] K. Miyokawa, S. Saito, T. Katayama, T. Satio, T. Kamino, K. Hanashima, Y. Suzuki, K. Mamiya, T. Koide, and S. Yuasa, Jpn. J. Appl. Phys. Part 2 **44**, L9 (2005).
[18] M. Sicot, S. Andrieu, F. Bertran, and F. Fortuna, Phys. Rev. B **72**, 144414 (2005).
[19] N. D. Telling, G. van der Laan, S. Ladak, and R. J. Hicken, Appl. Phys. Lett. **85**, 3803 (2004).
[20] J. Grabis, A. Bergmann, A. Nefedov, K. Westerholt, and H. Zabel, Phys. Rev. B **72**, 024437 (2005).
[21] S. Stadler, J. Appl. Phys. **97**, 10C302 (2005).
[22] M. Kallmayer, H. J. Elmers, B. Balke, S. Wurmehl, F. Emmerling, G. H. Fecher, and C. Felser, J. Phys. D **39**, 786 (2006).
[23] S. Wurmehl, G. H. Fecher, H. C. Kandpal, V. Ksenofontov, C. Felser, and H.-J. Lin, Appl. Phys. Lett. **88**, 032503 (2006).
[24] J. Schmalhorst, S. Kammerer, M. Sacher, G. Reiss, A. Hutten, and A. Scholl, Phys. Rev. B **70**, 024426 (2004).
[25] T. Saito, T. Katayama, T. Ishikawa, M. Yamamoto, D. Asakura, and T. Koide, Appl. Phys. Lett. **91**, 262502 (2007).
[26] T. Saito, T. Katayama, A. Emura, N. Sumida, N. Matsuoka, T. Ishikawa, T. Uemura, M. Yamamoto, D. Asakura, and T. Koide, J. Appl. Phys. **103**, 07D712 (2008).
[27] D. Asakura, T. Koide, S. Yamamoto, K. Tsuchiya, T. Shioya, K. Amemiya, V. R. Singh, T. Kataoka, Y. Yamazaki, Y. Sakamoto, A. Fujimori, T. Taira, and M. Yamamoto, Phys. Rev. B **82**, 184419 (2010).
[28] G.-f. Li, Y. Honda, T. Taira, K.-i. Matsuda, T. Uemura, M. Yamamoto, Y. Miura, and M. Shirai (unpublished).
[29] W. Kohn and N. Rostoker, Phys. Rev. B **94**, 1111 (1954).
[30] H. Akai and P. H. Dederichs, Phys. Rev. B **47**, 8739 (1993).
[31] M. Rasolt and D. J. W. Geldart, Phys. Rev. B **34**, 1325 (1986).
[32] C. T. Chen, Y. U. Idzerda, H.-J. Lin, N. V. Smith, G. Meigs, E. Chaban, G. H. Ho, E. Pellegrin, and F. Sette, Phys. Rev. Lett. **75**, 152 (1995).
[33] K. Miyamoto, K. Iori, A. Kimura, T. Xie, M. Taniguchi, S. Qiao, and K. Tsuchiya, Solid State Commun. **128**, 163 (2003).
[34] K. Amemiya, Phys. Chem. Chem. Phys. **14**, 10477 (2012).
[35] K. Amemiya, S. Kitagawa, D. Matsumura, H. Abe, T. Ohta, and T. Yokoyama, Appl. Phys. Lett. **84**, 936 (2009).
[36] B. T. Thole, P. Carra, F. Sette, and G. van der Laan, Phys. Rev. Lett. **68**, 1943 (1992).
[37] P. Carra, B. T. Thole, M. Altarelli, and X. Wang, Phys. Rev. Lett. **70**, 694 (1993).
[38] Y. Teramura, A. Tanaka, and T. Jo, J. Phys. Soc. Jpn. **65**, 1053 (1996).
[39] I. Galanakis, P. H. Dederichs, and N. Papanikolaou, Phys. Rev. B **66**, 174429 (2002).
[40] S. Hakamata, T. Ishikawa, T. Marukame, K.-i. Matsuda, T. Uemura, M. Arita, and M. Yamamoto, J. Appl. Phys. **101**, 09J513 (2007).
[41] F. M. F. de Groot, J. Electron Spectrosc. Relat. Phenom. **67**, 529 (1994).